# 9.5 ENSEMBLE STORM-SCALE DATA ASSIMILATION AND PREDICTION FOR SEVERE CONVECTIVE STORMS

David Dowell, Glen Romine, and Chris Snyder
National Center for Atmospheric Research*, Boulder, CO

## 1. INTRODUCTION

Numerical weather prediction and ensemble forecasting are considered important components of the process of issuing severe weather watches and warnings in the future (Stensrud et al 2009). However, considerable challenges remain in understanding and predicting the initiation and evolution of high impact convective weather events. Efforts to produce ensemble forecasts on the scale of convective storms with fully complex mesoscale models have just begun (e.g., Kong et al. 2007, Lei et al. 2009), and there are still significant opportunities for improving guidance from such storm-scale ensemble forecasts, particularly during the first few hours of the forecast.

To help us evaluate current and near-future capabilities in storm-scale ensemble prediction, we have developed an ensemble-based data-assimilation and prediction system with both mesoscale and storm-scale probabilistic analyses and forecasts, employing the Weather Research and Forecasting (WRF) model (Skamarock et al. 2008) and Data Assimilation Research Testbed (DART) tools (Anderson and Collins 2007, Anderson et al. 2009). We have taken advantage of previous experience with mesoscale (e.g., Fujita et al. 2007, Torn and Hakim 2008) and storm-scale (e.g., Aksoy et al. 2009, 2010; Dowell and Wicker 2009) ensemble-based data-assimilation and prediction systems when "putting the pieces together" for the current system. We are studying a retrospective period of 4-17 June 2009 with 3-hourly mesoscale (horizontal grid spacing $\Delta x$=15 km) ensemble analyses with continuous cycling on a continental United States (CONUS) domain (Fig. 1a), which provides initial and boundary conditions for regional storm-scale ($\Delta x$=3 km) analyses and forecasts centered near the Colorado Front Range (Fig. 1b). On the storm-scale domain, continuous assimilation of Doppler-velocity and "no-precipitation" (Aksoy et al. 2009) observations for one hour precedes ensemble forecasts out to six hours.

The Front Range domain supports the interest in the Short-Term Explicit Prediction (STEP) program at the National Center for Atmospheric Research (NCAR) in predicting convection initiation and evolution in the vicinity of complex terrain. The early-mid June 2009 retrospective period corresponds to a period of active weather and data collection by the Verification of the Origins of Rotation in Tornadoes Experiment 2 (VORTEX2). Among several VORTEX2 test cases selected for detailed study, two are discussed here: the 5 June 2009 Goshen County, WY tornadic supercell and the 11-12 June 2009 southeast CO nontornadic supercells. In subsequent sections, we describe the components of the WRF-DART mesoscale and storm-scale ensemble data-assimilation and prediction system and discuss initial results.

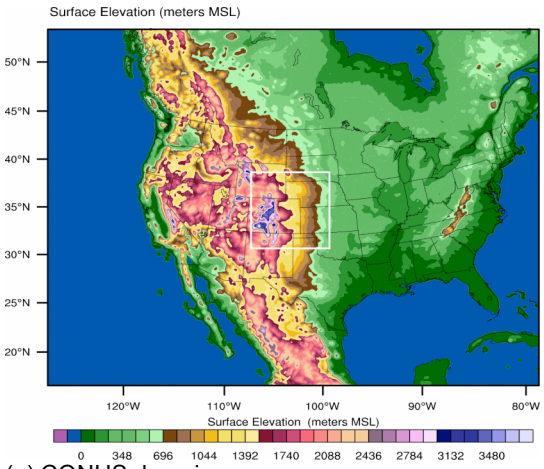


(a) CONUS domain

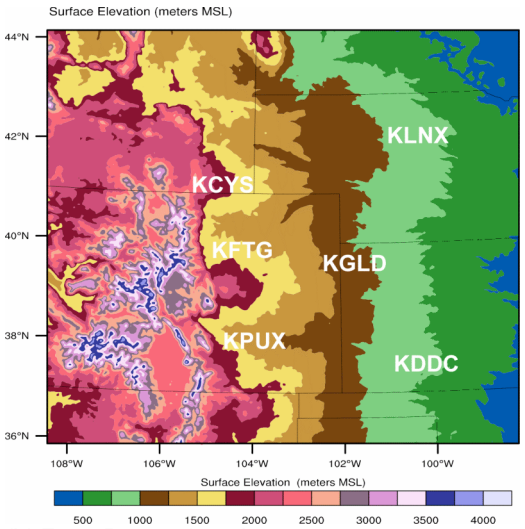


(b) Front Range domain

Figure 1. Surface elevation (shading; m MSL) in the WRF model in the (a) CONUS domain ($\Delta x$ = 15 km) and (b) Front Range domain ($\Delta x$ = 3 km).

* The National Center for Atmospheric Research is sponsored by the National Science Foundation.

*Corresponding author address:* David Dowell, National Center for Atmospheric Research, P. O. Box 3000, Boulder, CO 80307-3000, ddowell@ucar.edu

## 2. MESOSCALE DATA ASSIMILATION

Data-assimilation and forecasting experiments on both the CONUS and Front Range domains use WRF-ARW version 3.1.1, with bug fixes plus enhancements to output additional diagnostic fields (radar reflectivity, hydrometeor fall velocity, updraft helicity, etc.). The WRF model was configured as indicated in Table 1. To facilitate comparison of our results with those from real-time storm-scale forecasting systems (Weiss et al. 2010), we intentionally configured the WRF model similarly. For example, the Front Range domain uses the same horizontal grid spacing, vertical levels, PBL scheme, precipitation-microphysics scheme, and radiation scheme as NOAA's High-Resolution Rapid Refresh (HRRR) model.

| ***Model Parameter*** | ***CONUS*** | ***Front Range*** |
|---|---|---|
| Horizontal grid | $\Delta x$ = 15 km<br>369 × 297 points | $\Delta x$ = 3 km<br>301 × 301 points |
| Vertical grid | 51 levels<br>top level 65 mb | 51 levels<br>top level 65 mb |
| PBL scheme | MYJ | MYJ |
| Land surface | NOAH | NOAH |
| Microphysics | Thompson | Thompson |
| Convective scheme | Kain-Fritsch | none |
| Radiation | RRTM (longwave)<br>Dudhia (shortwave) | RRTM (longwave)<br>Dudhia (shortwave) |

Table 1. Summary of WRF model (Skamarock et al. 2008) configuration for the CONUS and Front Range domains.

The 50-member mesoscale ($\Delta x$=15 km) WRF ensemble mean was initialized with the Global Forecast System (GFS) analysis at 1200 UTC 31 May 2009. The initial ensemble and boundary conditions were then produced from random perturbations added to the ensemble mean using the WRF variational data-assimilation system (WRF-Var) "CV3" option. Boundary conditions for subsequent analysis times through 0000 UTC on 18 June 2009 were drawn from similarly perturbed GFS analyses valid every 6 hours, with interpolated intermediate boundary files every 3 hours. While it would have been more appropriate to use 3- and 6-h forecasts for the mesoscale boundary conditions, this simplification was not expected to have a significant impact on the storm-scale domain, which is well within the interior of the mesoscale domain. After several days of continuous cycling, the mesoscale ensemble does not depend significantly on the GFS initial conditions at 1200 UTC 31 May, but the GFS boundary conditions remain relevant throughout the period of interest. Adaptive prior spatially- and temporally-varying covariance inflation (Anderson 2009) was also used to maintain ensemble spread during the 18-day cycling period. Thus, sources of spread for our mesoscale ensemble are adaptive inflation, WRF-Var initial and boundary condition perturbations, and WRF model processes.

The DART software is used to assimilate conventional "mesoscale observations" into the WRF ensemble. This community tool is a parallel implementation of an ensemble adjustment Kalman filter adapted for geophysical data assimilation. DART works with various models, including the WRF model (Anderson and Collins 2007; Anderson et al. 2009). Ensemble Kalman filters use the statistics of a forecast ensemble to estimate the background-error covariances needed for data assimilation. Results of EnKF data assimilation provide a natural starting point for ensemble forecasting.

Most of the assimilated observations for the mesoscale domain come from NOAA's Meteorological Assimilation Data Ingest System (MADIS):

- radiosonde westerly wind component ($u$), southerly wind component ($v$), temperature ($T$), dewpoint ($T_d$), and altimeter setting ($p_{alt}$);
- surface $u$, $v$, $T$, $T_d$, and $p_{alt}$;
- marine (buoy) $u$, $v$, $T$, $T_d$, and $p_{alt}$; and
- aircraft $u$, $v$, $T$, and $T_d$.

Additional observations were drawn from NCEP BUFR archives: satellite cloud-track winds $u$ and $v$. The observations (approximately 80,000 observations per assimilation cycle) were assimilated every 3 hours. Prognostic variables that were updated are the 3 wind components; geopotential height; potential temperature; perturbation dry air mass; mixing ratios of water vapor, cloud, rain, ice crystals, snow, and graupel/hail; and intercept parameters of ice crystals and rain. The localization half width was 320 km (4 km) in the horizontal (vertical), and the localization function was the 5th order correlation function from Gaspari and Cohn (1999). Observation errors are specified similarly to those used by Torn and Hakim (2008). Observation likelihoods more than 3 ensemble standard deviations away from the prior ensemble mean are not assimilated.

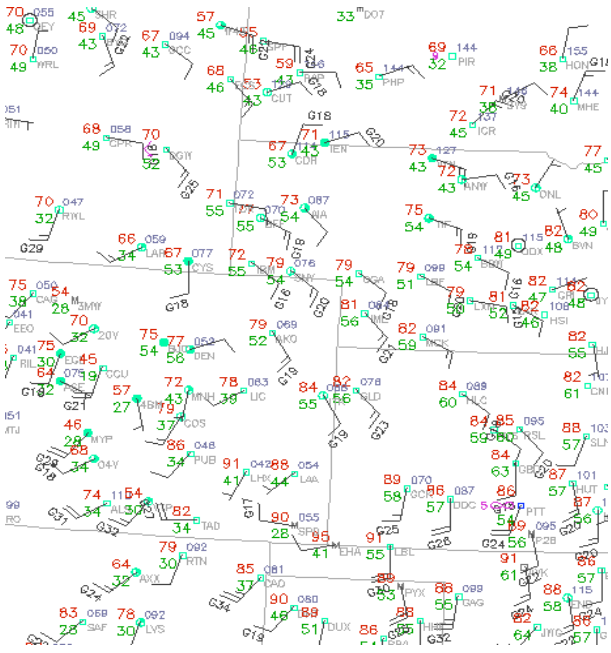

Figure 2. Surface observations (temperature in °F, dewpoint in °F, and wind in kt indicated in red, in green, and by barbs) at 2100 UTC 5 June 2009 (obtained in real time from www.rap.ucar.edu/weather/).

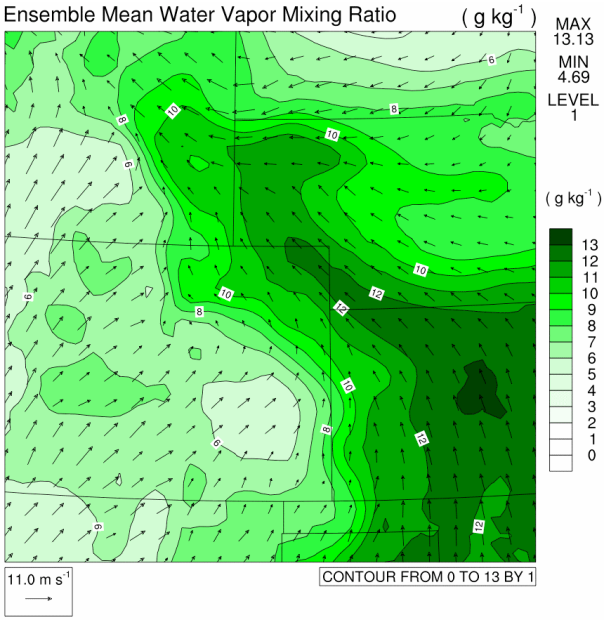


(a) Ensemble-mean water-vapor mixing ratio (contour interval 1.0 g kg$^{-1}$) and horizontal winds (vectors).

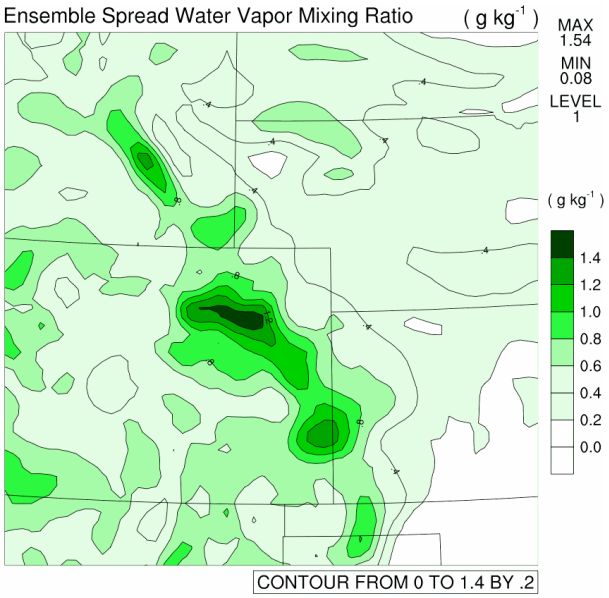


(b) Ensemble standard deviation of water-vapor mixing ratio (contour interval 0.2 g kg$^{-1}$).

Figure 3. Prior ensemble (3-h forecast) fields on the CONUS ($\Delta x$=15 km) grid at the lowest model level (approximately 8 m AGL) at 2100 UTC 5 June 2009.

An example case from 5 June 2009 is illustrated in Figs. 2 and 3. The surface map in the afternoon (Fig. 2) shows upslope southeasterly flow and mid 50 °F dewpoints on the high plains of northeast CO, the NE panhandle, and southeast WY. Model fields (Fig. 3) are for the 3-h ensemble forecast from 1800 to 2100 UTC 5 June, following cycling of the mesoscale ensemble continuously for nearly 5 days. Ensemble-mean water-vapor mixing ratio and horizontal winds at the lowest model level fairly resemble the observed surface pattern. The moist axis from west-central KS into northwest KS, through northeast CO, into the NE panhandle and southeast WY can be seen on the surface plot (Fig. 2) and in the WRF-DART ensemble-mean forecast (Fig. 3a), with the latter appearing to be smoother. Notably, a corridor of relatively low ensemble spread (which is equated to high confidence in an EnKF system) is forecast within this moist axis while relatively high spread (equated to low confidence) is indicated along the gradient on the southwest side of moist axis.

## 3. STORM-SCALE RADAR-DATA ASSIMILATION

For our "radar" storm-scale ensembles, we define $t_0$ as the time at which a storm-scale ensemble forecast begins. Initializing this ensemble begins with the mesoscale ensemble analysis at $t_0$ – 3 h, from which a 9-h mesoscale ensemble forecast is produced to provide boundary conditions for the duration of the storm-scale analysis and forecast window ($t_0$ – 3 h to $t_0$ + 6 h). Initial conditions for the nested storm-scale ensemble are made from one-way nesting from the 15-km CONUS (Fig. 1a) forecast valid at $t_0$ – 1 h, to the 3-km Front Range domain (Fig. 1b), with initial and boundary conditions drawn from a consistent mesoscale ensemble member.

Radar data are assimilated from 6 Weather Surveillance Radars - 1988 Doppler (WSR-88D) in the central high plains: KCYS, KFTG, KPUX, KLNX, KGLD, and KDDC (Fig. 1b) every 3 min from $t_0$ – 1 h to $t_0$. Two types of radar observations are assimilated: Doppler-velocity and "no-precipitation" observations (Aksoy et al. 2009). The latter are low values of radar reflectivity that indicate an absence of precipitation. Raw radar observations were first objectively analyzed at each elevation angle (e.g., Dowell and Wicker 2009), from each radar, to Cartesian gridpoints that are 6-km apart. Assimilating observations at this coarse resolution keeps the computation manageable and is appropriate given the relatively coarse horizontal grid resolution of the forecast model.

Automated quality-control algorithms were developed for processing the objectively-analyzed radar observations. Multi-day statistics for radar data at each elevation angle from each radar were used to identify locations of likely ground clutter, and data at these locations were deleted. Two types of ground clutter were flagged: (1) locally high terrain, identified by a high rate of reflectivity-data availability, low reflectivity standard deviation, low Doppler-velocity standard deviation, and mean Doppler velocity near zero and (2) highway traffic, identified by a high rate of reflectivity-data availability, low reflectivity standard deviation, and high Doppler-velocity standard deviation.

A simple but effective method was used to unfold aliased Doppler-velocity data. During the objective analysis, all

Doppler-velocity observations were forced to be within the same Nyquist-velocity bin (Miller et al. 1986). Then, each objectively-analyzed velocity observation was "unfolded", if necessary, right before it was assimilated into the storm-scale ensemble. That is, each velocity observation was unfolded into the Nyquist-velocity bin that minimized the difference between the observation and the prior ensemble-mean estimate of the observation.

Standard deviations of observation errors were specified as 2.0 m $s^{-1}$ and 2.0 dBZ for Doppler-velocity and "no-precipitation" observations, respectively. Observation likelihoods that weren't within 3 ensemble standard deviations of the prior ensemble mean (after unfolding, in the case of Doppler velocity) were not assimilated. The influence of each radar observation on the model state was localized with a half width of 12 km (6 km) in horizontal (vertical). As in the case of the mesoscale data assimilation, the 5th order Gaspari and Cohn (1999) correlation function was used for localization.

In addition to the spread that came from the mesoscale-ensemble initial and boundary conditions, localized additive noise (Dowell and Wicker 2009) provided additional spread to the storm-scale ensembles. The additive noise consisted of local, random perturbations to the horizontal wind components, temperature, and water vapor. The perturbations were smoothed so that they had length scales of 4 km (2 km) in the horizontal (vertical) (Dowell and Wicker 2009).

Since being proposed by Snyder and Zhang (2003), EnKF storm-scale radar-data assimilation techniques have been studied and refined mostly in simplified numerical models (e.g., Dowell et al. 2004; Tong and Xue 2005; Dowell and Wicker 2009; Aksoy et al. 2009, 2010). Only recently have experiments begun with EnKF radar-data assimilation in fully complex mesoscale models (e.g., Lei et al. 2009). Improving storm-scale ensemble design in fully complex models will require continued experimentation. Currently, we are experimenting with using spatially- and temporally-varying adaptive inflation to increase spread in the storm-scale ensembles. The 11-12 June case was run with DART adaptive inflation turned on, and the 5 June case was run with adaptive inflation turned off. The result is different behavior to the ensemble spread in the two cases (Fig. 4).

The prior and posterior diagnostic statistics for assimilated Doppler-velocity observations that are shown in Fig. 4 for the two cases are: (red) root-mean square of innovations (RMSI), where innovation = observation – forecast or observation – analysis; (green) mean of forecast – observation or analysis – observation; and (blue) total spread = square root of the summed ensemble variance and observation-error variance. One encouraging result is that the statistics become steady from about 20-30 min through the end of the data-assimilation window. Another encouraging result is that the mean differences between the model's estimates of the observations and the observations themselves (green) are close to zero.

The differences between the prior and posterior spread are, on average, greater in the 11-12 June case (blue sawtooth pattern in Fig. 4b) than in the 5 June case (Fig. 4a) since adaptive inflation was turned on in the former case but not in the latter. One characteristic of a well-designed ensemble is that the "consistency ratio" of total spread to RMSI should be roughly 1 (Dowell et al. 2004). The consistency ratio in these two cases is typically somewhat greater than 1. For the 5 June case, forecast RMSI was often less than the assumed observation error (Fig. 4a), meaning that on average, the observations were being under fit.

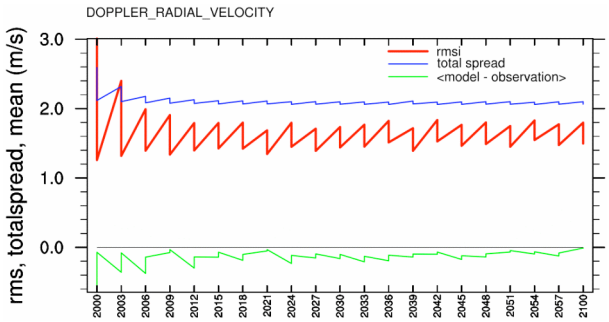


(a) 2000 to 2100 UTC 5 June 2009.

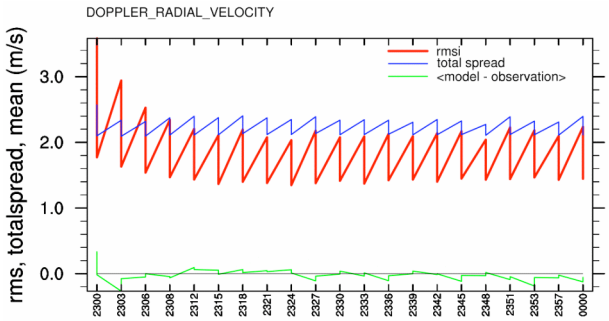


(b) 2300 UTC 11 June to 0000 UTC 12 June 2009.

Figure 4. Prior and posterior observation-space diagnostic statistics [m $s^{-1}$; root-mean square of the innovations, "total spread" (explained in text), and mean of forecast/analysis minus observations shown in red, blue, and green, respectively] for Doppler velocity during the 1-h assimilation window. Times (UTC) are indicated on the bottom axis.

## 4. STORM-SCALE ENSEMBLE FORECASTING

For the "radar" ensembles, 6-hour ensemble forecasts are produced from $t_0$ to $t_0$ + 6 h following the 1-hour radar-data assimilation. To allow interpretation of the "impact" of assimilation of radar observations on forecast performance, "control" storm-scale ensemble forecasts are made which are the same as "radar", except radar data are not assimilated from $t_0$ – 1 hour to $t_0$. That is, a free forecast is made on the nested Front Range domain

from $t_0$ – 1 h to $t_0$ + 6 h. Examples of ensemble forecasts for the 5 June and 11-12 June cases are shown in Figs. 5-8. One helpful parameter for identifying the model equivalent of supercell storms is updraft helicity (Kain et al. 2008). This field represents the vertical integral of the product of vertical velocity and the vertical component of vorticity from 2-5 km AGL, and highlights lower to middle tropospheric cyclonically rotating updrafts. Results of ensemble forecasts are conveyed here in terms of probability of updraft helicity exceeding 75 $m^2$ $s^{-2}$ during the 6-h (7-h) "radar" ("control") ensemble forecast.

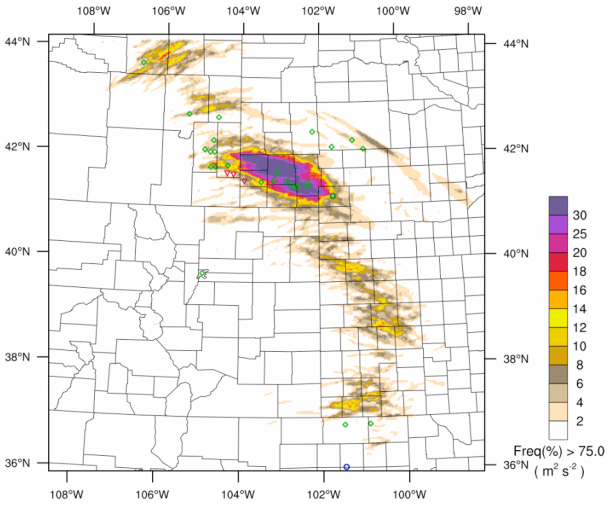


(a) "Control" ensemble forecast from 2000 UTC 5 June to 0300 UTC 6 June 2009.

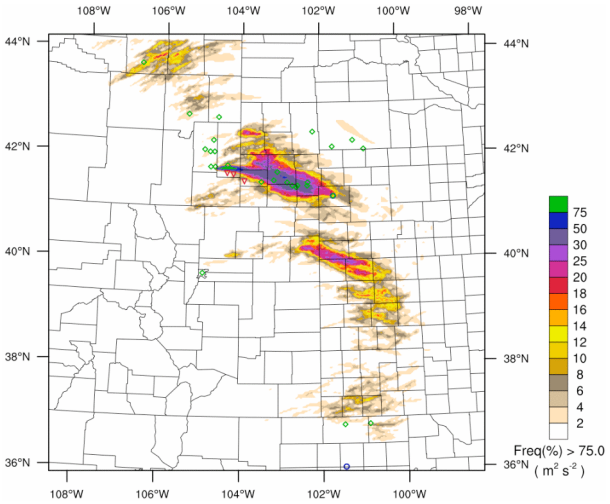


(b) "Radar" ensemble forecast from 2100 UTC 5 June to 0300 UTC 6 June 2009.

Figure 5. Ensemble probability (%; shading) of updraft helicity exceeding 75 $m^2$ $s^{-2}$ during the forecast period. SPC preliminary storm reports (tornadoes in red, hail in green, strong winds in blue) are also shown.

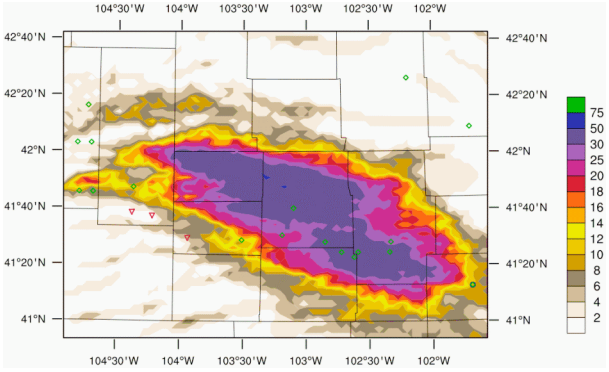


(a) "Control" ensemble forecast.

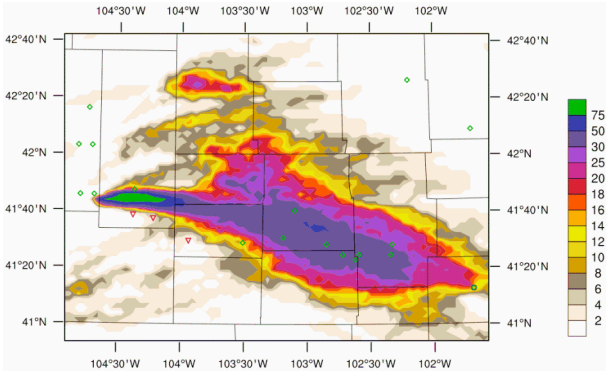


(b) "Radar" ensemble forecast.

Figure 6. As in Fig. 5, except zoomed in on the southeast WY - NE panhandle region.

On a broad scale, "control" and "radar" ensemble forecasts for the 5 June case are rather similar (Fig. 5). In these experiments, mesoscale data assimilation, not storm-scale radar-data assimilation, seems to determine mesoscale regions where rotating storms develop in the forecast. Radar-data assimilation changes smaller-scale details (Fig. 6).

For the June 5 and June 11-12 "radar" ensemble forecasts, there is a good correspondence between swaths of predicted high probabilities of rotating updrafts and swaths of severe weather reports from observed supercells (Figs. 5b, 6b, 7, and 8). The predicted swaths are biased somewhat to the left of the observed severe weather, as discussed in the following section. For the June 5 case, a swath of relatively high probability from northeast CO into northwest KS (Fig. 5) corresponds to an event that didn't happen. With only two cases, we can't determine if probabilities are reliable. However, changes resulting from radar-data assimilation do make sense. A comparison of the "control" to the "radar" forecast (Fig. 6) indicates that the additional information from the radar data has sharpened the probabilistic forecast, that is, increased the maximum probability and narrowed the swath of high probabilities.

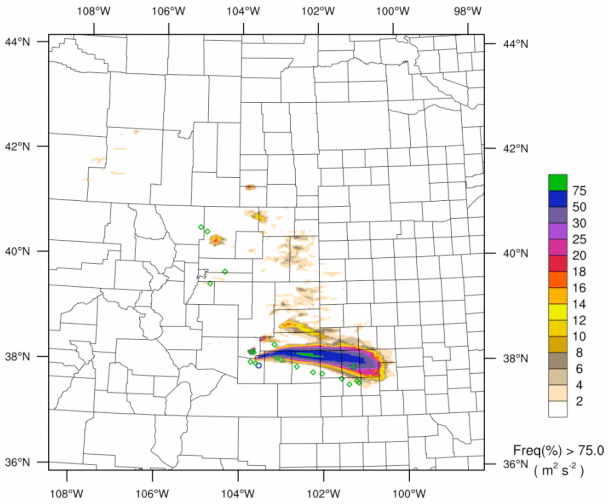


Figure 7. As in Fig. 5, except for the "radar" ensemble forecast between 0000 and 0600 UTC 12 June 2009.

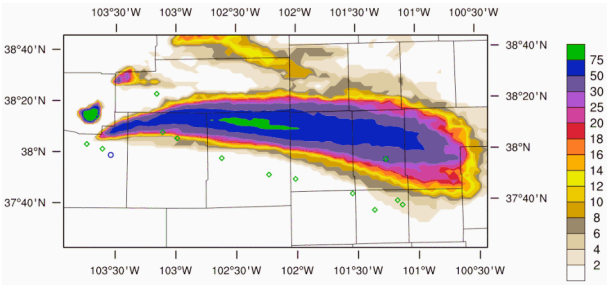


Figure 8. As in Fig. 7, except zoomed in on the southeast CO - southwest KS region.

Other criteria we are using to evaluate the storm-scale forecasts are whether storms evolve smoothly from the analysis to the forecast and whether there is a correspondence between observed and predicted storm locations for individual members. Updraft locations at 30-min intervals from the analysis to the 1.5-h forecast are shown in Fig. 9 for ensemble member 1 in the June 11-12 case. Corresponding observed radar-reflectivity images at the same times are shown in Fig. 10. Early in the forecast, the southernmost updraft ("A" in Fig. 9) strengthened rapidly and merged with updraft "B". The net effect was a discrete southeastward storm propagation, and inspection of the ensemble forecast (Fig. 8) suggests that all members depicted a similar evolution. In agreement with the model forecast, the observed southernmost storm "A" did strengthen early in the forecast period, as indicated by an increase in reflectivity (Figs. 10a and b). However, unlike in ensemble member 1, the southernmost two storms "A" and "B" maintained separate identities for at least ~1 h of the forecast period shown. This result could highlight resolution limitations of our ensemble. The 3-km horizontal grid spacing could be insufficient to simulate interacting storms in such close proximity.

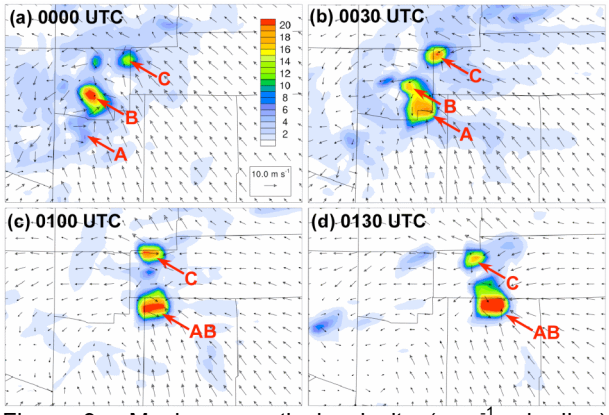


Figure 9. Maximum vertical velocity (m $s^{-1}$; shading) within the grid column during the previous 15 min and horizontal winds at 10 m AGL (m $s^{-1}$; vectors) for ensemble member 1 at four different times: (a) 0000 UTC (analysis time), (b) 0030 UTC, (c) 0100 UTC, and (d) 0130 UTC (1.5 h forecast) 12 June 2009.

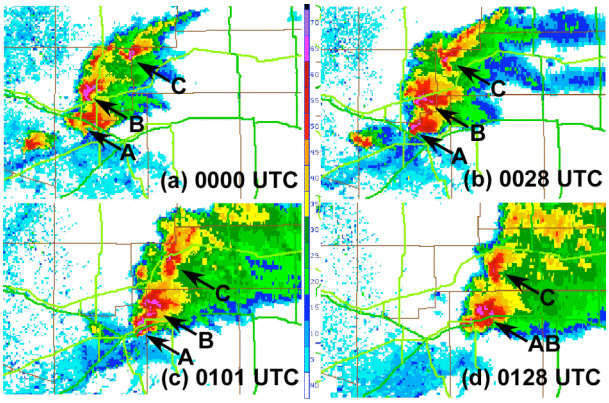


Figure 10. KPUX radar reflectivity factor (dBZ; shading) at 0.5° elevation angle at four times: 0000, 0028, 0101, and 0128 UTC 12 June 2010. Images obtained from catalog.eol.ucar.edu/vortex2_2009.

## 5. DISCUSSION

We are currently producing storm-scale ensemble forecasts for more cases during the 4-17 June 2009 retrospective period. Initial results for the June 5 and 11 cases are encouraging in several ways. Cycling the mesoscale ensemble continuously for the two-week period appears to be producing adequate initial and boundary conditions for storm-scale forecasts, even though the mesoscale ensemble is only being provided a subset of the observations that operational models such as the NAM, GFS, and RUC assimilate. Another encouraging result is that the ensembles produced swaths of high forecast probabilities of rotating updrafts near the most significant observed supercell storms in the two cases. Radar-data assimilation sharpened the probabilistic forecast on 5 June 2009, increasing the maximum probability and narrowing the swath of high probabilities. Furthermore, storms in the ensemble

members evolve rather smoothly from the end of the radar-data-assimilation window into the free forecast.

Evidence in initial results suggests that we will have to explore ways to introduce more diversity into the storm-scale ensemble forecasts. In both cases (Figs. 6 and 8), swaths of rotating storms in the ensemble were biased to the left of observed swaths of severe weather. We speculate that one factor is the coarse grid spacing, which could be insufficient to adequately represent storm processes related to observed rightward storm propagation. Supporting this speculation is the inability of all ensemble members to maintain two separate updrafts in close proximity at the south end of the storm line on 12 June 2009 (Figs. 8-10). Another factor in the leftward bias of the predicted storm tracks could be that the simulated cold pools are too weak in these cases.

Producing reliable ensemble forecasts on the convective-storm scale remains very challenging. Nevertheless, results from experiments such as these provide helpful guidance in the development of storm-scale ensemble techniques.

## ACKNOWLEDGMENTS

This work was supported by a grant from the US Weather Research Program - Short-Term Explicit Prediction (STEP) program. We thank Jenny Sun for her leadership of the STEP program and the data-assimilation component. We appreciate the support of the DART system by Jeff Anderson, Nancy Collins, and Tim Hoar. Ryan Torn and Soyoung Ha provided helpful guidance in configuring the mesoscale WRF-DART system and observation preprocessors. We thank Greg Thompson for providing WRF precipitation-microphysics code along with reflectivity and fall-velocity calculations, Scott Dembek for providing diagnostic output routines, and Curtis Alexander for sharing information about the High Resolution Rapid Refresh model. The National Center for Atmospheric Research is sponsored by the National Science Foundation.

## REFERENCES

Aksoy, A., D. C. Dowell, and C. Snyder, 2009: A multicase comparative assessment of the ensemble Kalman filter for assimilation of radar observations. Part I: Storm-scale analyses. *Mon. Wea. Rev.*, **137**, 1805-1824.

Aksoy, A., D. C. Dowell, and C. Snyder, 2010: A multicase comparative assessment of the ensemble Kalman filter for assimilation of radar observations. Part II: Short-range ensemble forecasts. *Mon. Wea. Rev.*, **138**, 1273-1292.

Anderson, J. L., 2009: Spatially and temporally varying adaptive covariance inflation for ensemble filters. *Tellus*, **61**, 72-83.

Anderson, J. L., and N. Collins, 2007: Scalable implementations of ensemble filter algorithms for data assimilation. *J. Atmos. Oceanic Technol.*, **24**, 1452-1463.

Anderson, J., T. Hoar, K. Raeder, H. Liu, N. Collins, R. Torn, and A. Avellano, 2009: The Data Assimilation Research Testbed: A community facility. *Bull. Amer. Meteor. Soc.*, **90**, 1283-1296.

Dowell, D. C., and L. J. Wicker, 2009: Additive noise for storm-scale ensemble data assimilation. *J. Atmos. Oceanic Technol.*, **26**, 911-927.

Dowell, D. C., F. Zhang, L. J. Wicker, C. Snyder, and N. A. Crook, 2004: Wind and temperature retrievals in the 17 May 1981 Arcadia, Oklahoma, supercell: Ensemble Kalman filter experiments. *Mon. Wea. Rev.*, **132**, 1982-2005.

Fujita, T., D. J. Stensrud, and D. C. Dowell, 2007: Surface data assimilation using an ensemble Kalman filter approach with initial condition and model physics uncertainties. *Mon. Wea. Rev.*, **135**, 1846-1868.

Gaspari, G., and S. E. Cohn, 1999: Construction of correlation functions in two and three dimensions. *Quart. J. Roy. Meteor. Soc.*, **125**, 723-757.

Kain, J. S., S. J. Weiss, D. R. Bright, M. E. Baldwin, J. L. Levit, G. W. Carbin, C. S. Schwartz, M. L. Weisman, K. K. Droegemeier, D. B. Weber, and K. W. Thomas, 2008: Some practical considerations regarding horizontal resolution in the first generation of operational convection-allowing NWP. *Wea. Forecasting*, **23**, 931-952.

Kong, F., K. K. Droegemeier, and N. L. Hickmon, 2007: Multiresolution ensemble forecasts of an observed tornadic thunderstorm system. Part II: Storm-scale experiments. *Mon. Wea. Rev.*, **135**, 759-782.

Lei, T., M. Xue, and T. Yu, 2009: Multi-scale analysis and prediction of the 8 May 2003 Oklahoma City tornadic supercell storm assimilating radar and surface network data using EnKF. Preprints, *13th Conf. on Integrated Observing and Assimilation Systems for Atmosphere, Oceans, and Land Surface (IOAS-AOLS)*, Phoenix, AZ, Amer. Meteor. Soc., 6.4.

Miller, L. J., C. G. Mohr, and A. J. Weinheimer, 1986: The simple rectification to Cartesian space of folded radial velocities from Doppler radar sampling. *J. Atmos. Oceanic Technol.*, **3**, 162-174.

Skamarock, W. C., J. B. Klemp, J. Dudhia, D. O. Gill, D. M. Barker, M. G. Duda, X.-Y. Huang, W. Wang, and J. G. Powers, 2008: A description of the Advanced Research WRF Version 3. NCAR Technical Note TN-475+STR, 113 pp., available from www.mmm.ucar.edu/wrf/users/docs/arw_v3.pdf.

Snyder, C., and F. Zhang, 2003: Assimilation of simulated Doppler radar observations with an ensemble Kalman filter. *Mon. Wea. Rev.*, **131**, 1663-1677.

Stensrud, D. J., M. Xue, L. J. Wicker, K. E. Kelleher, M. P. Foster, J. T. Schaefer, R. S. Schneider, S. G. Benjamin, S. S. Weygandt, J. T. Ferree, and J. P. Tuell, 2009: Convective-scale warn-on-forecast system. A vision for 2020. *Bull. Amer. Meteor. Soc*., **90**, 1487-1499.

Tong, M., and M. Xue, 2005: Ensemble Kalman filter assimilation of Doppler radar data with a compressible nonhydrostatic model: OSS experiments. *Mon. Wea. Rev*., **133**, 1789-1807.

Torn, R. D., and G. J. Hakim, 2008: Performance characteristics of a pseudo-operational ensemble Kalman filter. *Mon. Wea. Rev*., **136**, 3947-3963.

Weiss, S. J., and co-authors, 2010: An overview of the 2010 NOAA Hazardous Weather Testbed spring forecasting experiment. *25th Conf. on Severe Local Storms*, Denver, CO, Amer. Meteor. Soc, presentation 7B.1.